International Forum on Aeroelasticity and Structural Dynamics
IFASD 2024
17-21 June 2024, The Hague, The Netherlands

ACTIVE FLUTTER SUPPRESSION AND GUST LOAD ALLEVIATION OF WINGS INCORPORATING FLOATING WINGTIPS

William Mansey[1], Fintan Healy[1], Huaiyuan Gu[1], Djamel Rezgui[1], Jonathan Cooper[1]

[1] School of Civil, Aerospace and Design Engineering, University of Bristol, UK

nd21650@bristol.ac.uk, fintan.healy@bristol.ac.uk, huaiyuan.gu@bristol.ac.uk,
djamel.rezgui@bristol.ac.uk, j.e.cooper@bristol.ac.uk

Keywords: Flared Folding Wingtips, Flutter, Active Control, Flutter Suppression

Abstract: In this paper, a two degree of freedom mathematical model was used to analyse active flutter suppression on wings featuring flared folding wingtips, via an additional control surface on the wingtip. The active control system took the wingtip fold angle as the input parameter. Using a proportional controller gain, the flutter onset speed could be increased by 25%, and a proportional controller can also be used to recreate the effect of a flare angle. Using a derivative controller, it was found that flutter could be prevented across all reasonable airspeeds. Both benefits could be realised without a significant change in the gust load alleviation provided by the flared folding wingtip. However, the control surface angular rates required to achieve flutter suppression were very high under certain conditions. If these control surface velocities are limited to realistic values, then the controller can no longer suppress the growth of instabilities for larger gust amplitudes.

1 INTRODUCTION

The induced drag created by a fixed wing aircraft can be reduced by increasing aspect ratio, providing a clear incentive to increase the wingspan of civilian aircraft. The limits imposed by standard aircraft gate sizes have recently been overcome in aircraft such as the Boeing 777X by using ground folding wingtips, where the wingtips are folded up while on the ground but are locked in position before take-off. However, the aspect ratio of this aircraft is still limited by the greater load as wingspan increases, and the consequent weight penalty [1].

One of the major structural requirements for aircraft wings is for them to be able to withstand gust loads, which are typically modelled using a series of 1-cosine gusts across a variety of gust lengths [2]. One possible solution to reduce the loads experienced during gust encounters is flared folding wingtips (FFWT). The presence of a flare angle produces a coupling between the angular rotation of the wingtip and the wingtip's angle of attack, which allows the FFWT to be used to reduce the peak loads experienced during a gust encounter, reducing the wing root bending moment, and therefore reducing the required wing weight [3].

One of the drawbacks of FFWTs is the introduction of a new mode of vibration, which can lead to the early onset of flutter. Flutter is the growth of an unstable mode of vibration caused by the interaction of the inertial, elastic, and aerodynamic forces above a critical onset speed. The growth of these violent oscillations can lead to structural failure; however, in certain instances the

exponential growth of these oscillations may be bounded by nonlinearities in the system, leading to limit cycle oscillations [4]. Wings featuring FFWTs are susceptible to flutter at speeds within the flight envelope, occurring primarily due to the coalescence of the FFWT and wing out of plane bending modes [5].

Previous research has investigated fitting the wingtip with an additional control surface, and statically varying the deflection angle of this tab has been shown to affect the flutter onset speed of the wing [6], however flutter was still encountered during some parts of the flight envelope. Applying prescribed sinusoidal deflections of this tab has also been previously researched and, if implemented correctly, this can further reduce the peak wing root bending moment associated with a gust encounter [7].

Another area of research is the use of active control for flutter suppression. This involves the use of a closed loop control system to suppress flutter when operating at speeds above the natural flutter onset speed, however this technology still lacks maturity and further research is needed before this can be adopted [8]. In addition, this research has not looked at applying these techniques to wings featuring FFWTs.

In this work, a numerical model is developed to examine the feasibility of using an active flutter suppression system on wings featuring FFWTs. In other words, the study will explore if using active tabs is a feasible solution to delay the low flutter onset speeds, which might be seen in wings featuring FFWTs. Furthermore, the effects of the use of an active flutter suppression system on the gust load alleviation provided by the FFWTs are also considered.

2 METHODOLOGY

A two degree-of-freedom (DoF) numerical model was created to model the aeroelastic behavior of the system, assuming a flexible inner wing and rigid flared folding wingtip. One DoF was used for the inner wing bending, represented as the inner wing tip deflection, and a second DoF was used for the wingtip fold angle. These were used as previous research indicated that the interaction between the wingtip flapping and inner wing bending mode was the primary flutter mechanism in systems incorporating FFWTs [5]. To validate the model, it is based off a wing used in previous research for experimental wind tunnel testing [6]. The numerical model was produced in MATLAB [9], and the ode45 solver, which uses a 4,5-Runga-Kutta method, was used for time domain simulations. Figure 1 shows the wing used in the previous experimental testing, and the definition of the inner wing, wingtip, and flare angle.

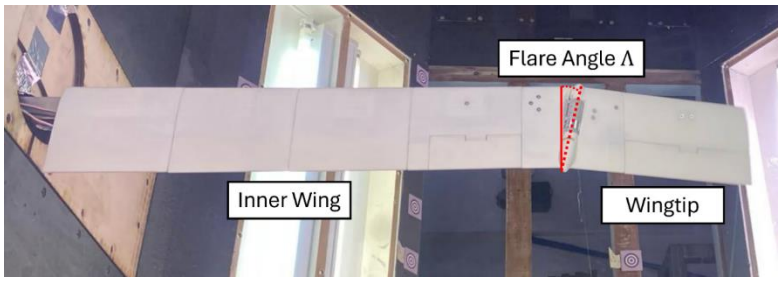

Figure 1: The wing used in the previous experimental testing [19].

2.1 Structural Model

The simplification to a 2 DoF model means that the structural model becomes a sprung pendulum, as shown in figure 2. m_{eq} is the inner wing mass, m_{WT} is the wingtip mass, and k_{eq} is the inner wing equivalent stiffness. z represents the tip deflection of the inner wing, and theta represents the fold angle of the wingtip, as shown in figure 2, where an upwards fold is defined as positive.

The aerodynamic forces are shown in grey. $F_{Z_{IW}}$ is the lift from the inner wing, $F_{Z_{WT}}$ is the vertical component of the wingtip lift forces, and M_θ is the moment from the lift acting on the wingtip.

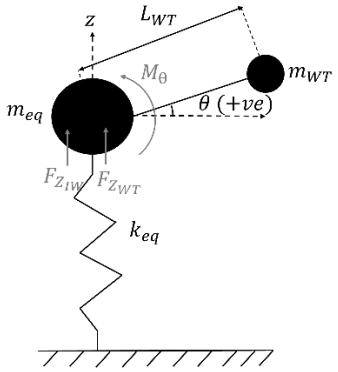

Figure 2: The 2 DoF structural model used to represent the wing, with aerodynamic forces shown in grey.

The value in the structural model for wingtip length (L_{WT}) is the distance from the tip of the inner wing to the centre of mass (COM) of the wingtip, which is assumed to be halfway along the wingtip. To determine the equivalent stiffness of the inner wing, it was assumed the load on the inner wing is approximately uniformly distributed, and therefore the inner wing stiffness can be calculated as

$$k_{eq} = \frac{8\, E_{eq}\, I_{eq}}{L_{IW}^3} \tag{1}$$

where E_{eq} is the inner wing spar's young's modulus, I_{eq} is the spar's second moment of area, and L_{eq} is its length. Equation 1 is derived by taking the equation for tip deflection under a uniformly distributed load [10], and then defining stiffness as the load required to obtain a deflection of 1m. The values used for the structural model are shown in Table 1 and come from the properties of the wing previously used for experimental testing [6].

Table 1: The values used for the structural model.

Wing Properties	Value
Inner Wing Mass M_{eq} (kg)	2.533
Wingtip Mass M_{eq} (kg)	0.563
Wingtip Moment of Inertia I_{WT} (kg m^2)	0.0067
Wingtip Length (to COM) L_{WT} (m)	0.1560
Inner Wing Equivalent Stiffness k_{WT} (N/m)	482.5

2.2 Dynamic Model

From the diagram in figure 2, the equations of motion of the system were then derived. The equations of motion take the form

$$\boldsymbol{M}\begin{bmatrix}\ddot{\boldsymbol{z}}\\ \ddot{\boldsymbol{\theta}}\end{bmatrix} = \boldsymbol{F} \tag{2}$$

The mass matrix can be determined by inspection of figure 2 where the z-direction inertial term is simply the sum of the two masses, and the theta inertial term can be determined to be $m_{WT}L_{WT}^2 + I_{WT}$, using the parallel axis theorem. The coupling term will then be the wingtip mass, multiplied by the horizontal distance away from the inner wing position. This leads to the 2x2 mass matrix such that

$$\boldsymbol{M} = \begin{bmatrix} m_{IW} + m_{WT} & m_{WT}L_{WT}cos\theta \\ m_{WT}L_{WT}cos\theta & m_{WT}L_{WT}^2 + I_{WT} \end{bmatrix} \tag{3}$$

To determine the force vector, a provision is made for the inclusion of the aerodynamic forces. The aerodynamic forces are returned as two values, a force in the z direction, which comes from a sum of the vertical force on both the wing and the wingtip, and a moment around the wingtip hinge due to wingtip lift. The remaining forces come from the weight of the two masses, the moment from the wingtip mass, the force from the wing stiffness, modelled as a spring, and finally a term to represent the force on the spring because of the wingtip rotating. The forces are the expressed in the force vector

$$\boldsymbol{F} = \begin{bmatrix} F_{z_{IW}} + F_{z_{WT}} + k_{IW}z - (m_{WT}L_{WT}sin\theta)\ddot{\theta} - m_{IW}g - m_{WT}g \\ M_\theta - m_{WT}gL_{WT}cos\theta \end{bmatrix} \tag{4}$$

To verify the derived equations of motion, they were compared to previous research that had modelled a flared folding wingtip in this way [11] and the equations were found to match. A python library, moyra [12], was then used to generate the initial MATLAB functions needed to carry out time domain simulations of these equations, and the basic stability analysis, described further in section 2.4.

2.3 Aerodynamic Model

The aerodynamic model used dimensions from the wing used in previous experimental testing [6], and these are shown in figure 3. The flare angle (Λ) is 10 degrees, and a NACA 0015 aerofoil is used.

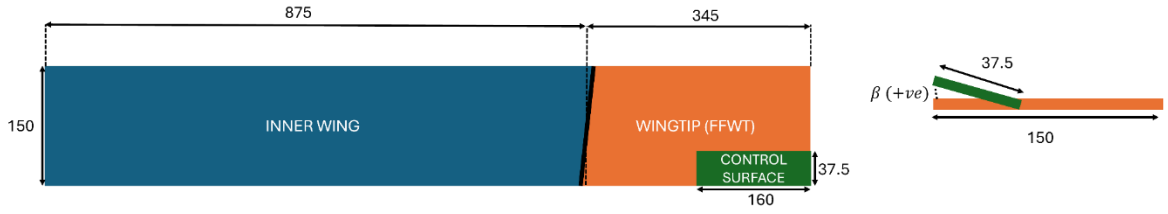

Figure 3: The dimensions of the wing used in the numerical model, with all dimensions in mm, and the sign convention for control surface deflection β.

To calculate the aerodynamic forces acting on the wing and the wingtip, the wing was split into two sections, the inner wing, and the wingtip. As the deflections of the folding wingtip are assumed to be relatively small, the fold angle is assumed not to influence the local lift in the inner wing section. Both the inner wing and wingtip were split into 50 equal width spanwise strips. As the wingtip is shorter than the inner wing, this results in a closer spacing on the wingtip. This is preferred, as the control surface means the variation in spanwise lift will be greater, and the wingtip moment is also used, not just the vertical lift, and therefore accurately placing the forces on the spanwise axis is more important on the wingtip.

To calculate the aerodynamic forces, the wing was modelled in XFLR 5 [13], and then 2D aerofoil analysis on the NACA 0015 aerofoil was carried out in the XFOIL direct analysis module. To model the 3D effects, a vortex lattice method (VLM) was used to generate a spanwise lift distribution. This was run at multiple angles of attack, and as expected, produced a linear relationship between angle of attack, and the local lift coefficient at each spanwise location. The data was processed to find the gradient (local lift curve slope), and then linear interpolation was used to calculate the local lift curve slope at the centre of each spanwise strip.

To model the effect of the control surface, its effect on the wing's lift was again examined in XFLR5. As shown in figure 3, a positive control surface deflection, β, is defined as an upwards control surface deflection. Under a VLM model, the effect of the control surface was to shift the zero-lift angle of attack but had no effect on the lift curve slope. The control surface primarily effected spanwise strips over the control surface but was still significant on those strips nearby to it, so these strips were also included when calculating the effect of control surface deflection. The effect of changing control surface deflection on the zero-lift angle of attack was again a linear relationship, meaning that the effect of the control surface could be calculated from the deflection angle and the rate of change of zero-lift angle of attack with respect to control surface deflection.

These results were all generated using the vortex lattice method, and therefore have the inherent limitations arising from that method. Of key relevance is the inability to predict where partially or fully detached flow will occur, and therefore the flow is assumed to be attached at all points [14]. This explains the completely linear relationships established and means that the model will not be valid at high local angles of attack, or at high control surface deflections. For this reason, the control surface was limited to maximum deflection angles of $\pm$ 30 degrees.

Finally, the effective angle of attack on the wingtip must be calculated. To account for the coupling between the wingtip fold angle and the angle of attack on the wingtip, it has been previously shown that

$$\Delta\alpha_{WT_{flare}} = -\arctan(\sin\theta \sin\Lambda) \tag{5}$$

can be used as an appropriate model if only small fold angles are considered [11]. The effective angle of attack also needs to consider the induced angle of attack from the motion of the two degrees of freedom. Using a small angle approximation, the change in angle of attack as a function of local vertical velocity, v, and forward flight velocity, U, can be approximated as

$$\Delta\alpha = -\frac{\dot{v}}{U} \tag{6}$$

For the wingtip, as this is assumed to be rigid, this relationship can be used to calculate the change in effective angle of attack at each spanwise strip as

$$\Delta\alpha_{WT_{induced}} = -\frac{\dot{z}}{U}cos\theta - \frac{\dot{\theta}y_{fwt}}{U} \tag{7}$$

Where the first terms represents the induced angle of attack due to the plunging motion of the hinge and the second term represents that due to the folding of the wingtip about the hinge. The structural model only captures the tip deflection, and therefore to get a better estimation of the induced velocity from bending across the entire wing, an assumed shape is used. As it is assumed that the load is approximately uniformly distributed along the wing, the following shape can be used [15],

$$\Delta\alpha_{IW_{induced}} = -\frac{\dot{z}}{U}\left(2y_{norm}^2 - \frac{4}{3}y_{norm}^3 + \frac{1}{3}y_{norm}^4\right) \tag{8}$$

where y_{norm} is the normalised position along the wing ($\frac{y}{L_{IW}}$). The relationship between upwards force and tip deflection assumes a uniform distribution, but this is clearly not the case for this load, and hence this force must be scaled appropriately. To choose an appropriate scale factor, the results when using the unscaled force were compared to previous experimental data [6], and a scale factor of 0.375 was found to provide a good match to the data shown in figure 4. The overall angles of attack for positions on the inner wing and wingtip are shown respectively in equations 9 and 10 [11].

$$\alpha_{IW}(y_{norm}) = \alpha_0 + \alpha_{IW_{induced}}(y_{norm}) \tag{9}$$

$$\alpha_{WT}(y_{fwt}) = \alpha_0\cos\theta + \alpha_{WT_{flare}} + \alpha_{WT_{induced}}(y_{fwt}) \tag{10}$$

2.4 Stability Analysis

To determine the natural frequencies, and damping ratios under a given airspeed, angle of attack and controller settings, the equilibrium position was first calculated for these conditions. For linear stability analysis, a linear model was created around the equilibrium position for those conditions, the Jacobian of this linear model was determined, and the eigenvalues and eigenvectors of the Jacobian were then calculated. The natural frequencies and damping ratios could then be found.

Additionally, time domain simulations were used, and in these simulations time domain simulations, the output was inspected for stability.

2.5 Gust Model

As part of the project, the wing's response to discrete gust loads was analysed, and these were modelled using the method set out in EASA CS-25 [16]. The model specified in these specifications, and used in this project, is set out in equations (11) and (12) below. The load alleviation factor, F_g, is assumed to be 1. U_{ref} is designated as the peak vertical velocity of the gust, H is the gust length, and s is the distance into the gust.

$$U_{ds} = U_{ref}F_g\left(\frac{H}{107}\right)^{\frac{1}{6}} \tag{11}$$

$$U_z = \frac{U_{ds}}{2}[1 - \cos(\frac{\pi s}{H})] \quad \text{for } 0 \le s \le 2H$$
$$U_z = 0 \quad \text{for } s > 2H \tag{12}$$

2.6 Controller Model

A wingtip tab controller was investigated using both a derivative gain, K_d, and a proportional gain, K_p, for the target control surface deflection.

Assuming a desired wingtip deflection of zero degrees, the error term used to drive the controller was equal to $-\theta$. Therefore, the control function was defined as

$$\beta_{target} = -K_p\theta - K_d\dot{\theta} \tag{13}$$

where β_{target} is the target control surface deflection in degrees. The possible target deflections were capped at $\pm$ 30 degrees. Initially, an ideal control surface actuator was modelled, meaning that the control surface deflection was always exactly equal to the target control surface deflection.

Clearly this is not a true assumption, so a simple control surface model was built into the simulation. This involved adding a third degree of freedom for the control surface deflection, β, which was modelled as an angular spring, of stiffness k_t, and damper, with damping coefficient c_t, with a second moment of inertia I_t. This results in the 3x3 mass matrix

$$\mathbf{M} = \begin{bmatrix} m_{IW} + m_{WT} & m_{WT}L_{WT}cos\theta & 0 \\ m_{WT}L_{WT}cos\theta & m_{WT}L_{WT}^2 + I_{WT} & 0 \\ 0 & 0 & I_t \end{bmatrix} \tag{14}$$

and updated force vector

$$\boldsymbol{F} = \begin{bmatrix} F_{z_{IW}} + F_{z_{WT}} + k_{IW}z - (m_{WT}L_{WT}sin\theta)\ddot{\theta} - m_{IW}g - m_{WT}g \\ M_\theta - m_{WT}gL_{WT}cos\theta \\ k_t\beta + c_t\dot{\beta} \end{bmatrix} \tag{15}$$

The first method to develop a more realistic model for a control surface involved implementing a model for a control surface actuator. There has been previous research on active flutter suppression systems, although not related to flared folding wingtips, that have instead used a transfer function to model a control surface actuator [18]. Therefore, the transfer function developed in this previous research,

$$G(s) = \frac{96710}{s^2 + 840s + 96710} \tag{16}$$

was also implemented, as this represents a model for an actuator suitable for active flutter suppression. By carrying out a reverse Laplace transform, the coefficients can be determined for the mass, spring, damper system implemented into the FFWT model, and these are shown in table 2.

However, these both this and the ideal control surface actuator allow unlimited angular velocities, so the second method to simulate a more realistic control surface was to prescribe a rate limit for the controller, specifying the maximum angular velocity the control surface can obtain. A rate of 50 deg/sec was chosen to be suitable maximum angular velocity. To ensure that this was the only significant change effecting the system, values for I_t, k_t and c_t had to be chosen that ensured that at the frequencies used, there was no noticeable difference between the demanded and performed control surface response before the rate limit was imposed. This was achieved by selecting values such that the damping ratio of this mode would be close to critically damped (0.95), and that the damped natural frequencies would be significantly higher than the oscillations present in the control surface demand. These values were then checked by running simulations to ensure that there was no discernible difference between the response and demand. The values used are presented in table 2 below.

Table 2: The coefficients used to model both the rate limited model, and the actuator transfer function model.

	Actuator Transfer Function Model	**Rate Limited Model**
I_t	1 / 96710	0.00001
k_t	1	1
c_t	840 / 96710	0.006008

The rate limit was then installed into the code and was enforced by capping the maximum ‘control force’ applied to the system to be that required to obtain a velocity of 50 deg/sec, based on the spring stiffness. As the second moment of inertia, I_t, is comparatively small, it was considered negligible in this calculation. To achieve this, the numerical ode solver method had to be changed to one with a constant time-step rather than variable time step. A first order Euler method was used, using the MATLAB function ode1 [17], and a time-step of 0.1ms was selected, as this produced almost identical results to the ode45 solver used before, and still ran simulations in a reasonable time. When the rate limit is imposed, using the model developed, modelling can only be done in the time domain, as the methods previously used to find the natural frequencies and damping ratios will no longer be valid.

3 RESULTS AND DISCUSSION

3.1 Model Evaluation

First, simulations were run to validate the numerical model. As the model is of a wing analysed in previous research, a simulation was conducted to recreate the numerical results shown in earlier research [6], which were generated with a more sophisticated model for inner wing bending. The variation in the natural frequencies and damping ratios with velocity, for the two numerical models, at an angle of attack of 2.5 degrees, is shown in figure 4. As airspeed changes, the

equilibrium tip deflection and fold angle vary, and hence the equilibrium position that the model is linearized around to calculate these natural frequencies and damping ratios are calculated also varies. The equilibrium position as airspeed is varied is shown in figure 5.

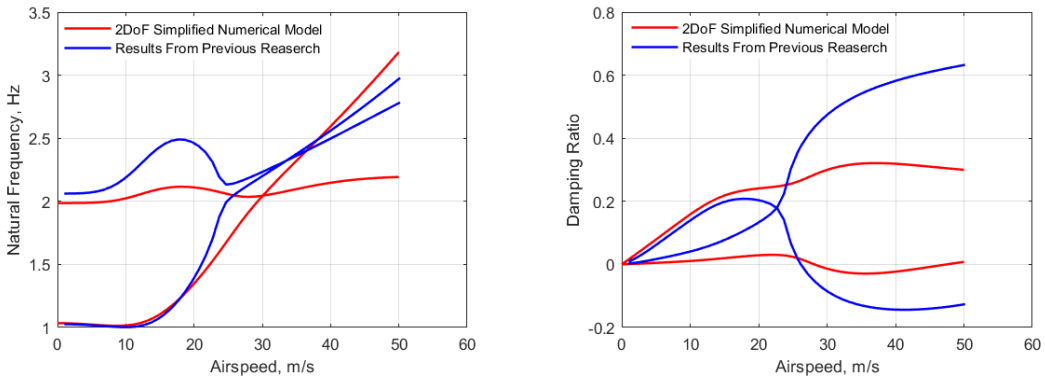

Figure 4: The natural frequencies and damping ratios of the wing at a 2.5 degrees angle of attack.

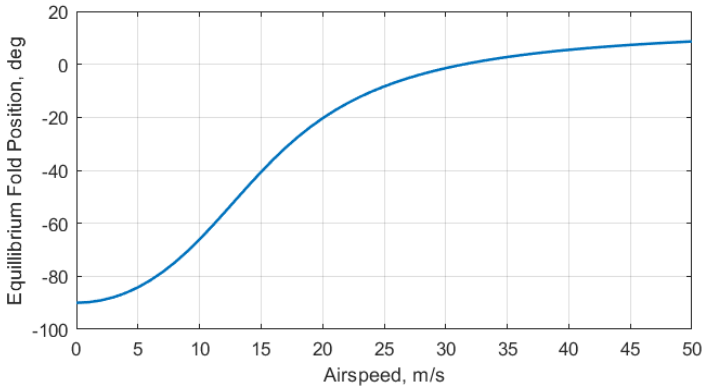

Figure 5: The equilibrium wingtip fold angle as airspeed is varied at a constant 2.5-degree angle of attack.

Comparing these to results from the previous research [6], they are mostly similar, however there are some differences. When comparing the trend in natural frequencies, the results are similar up until the intersection airspeed, and these frequencies intersect at the expected location. The major difference with the natural frequencies is the modes fail to coalesce at airspeeds above this intersection point, and therefore the behaviour at speeds significantly above the peak flutter speed are not accurately modelled. This is unsurprising given the relative simplicity of the numerical model used and is not a particularly relevant region for this study. The damping ratios individually show the expected behaviour as flight speed increases; however, they are quantitatively somewhat different, with the changes in the values less pronounced than those seen in previous reaserch. Again, these differences are expected due to the 2DoF simplification, and both models predict very similar flutter onset speeds, at a speed slightly below where the natural frequencies of the two modes cross.

The sensitivity of the model to two key parameters was also measured, the inner wing stiffness and the wingtip mass. The effect on changing these parameters on the natural frequencies and

damping ratios of the model was examined and are shown in figure 6 below. The angle of attack was fixed at 2.5 degrees, and the airspeed at 25 m/s.

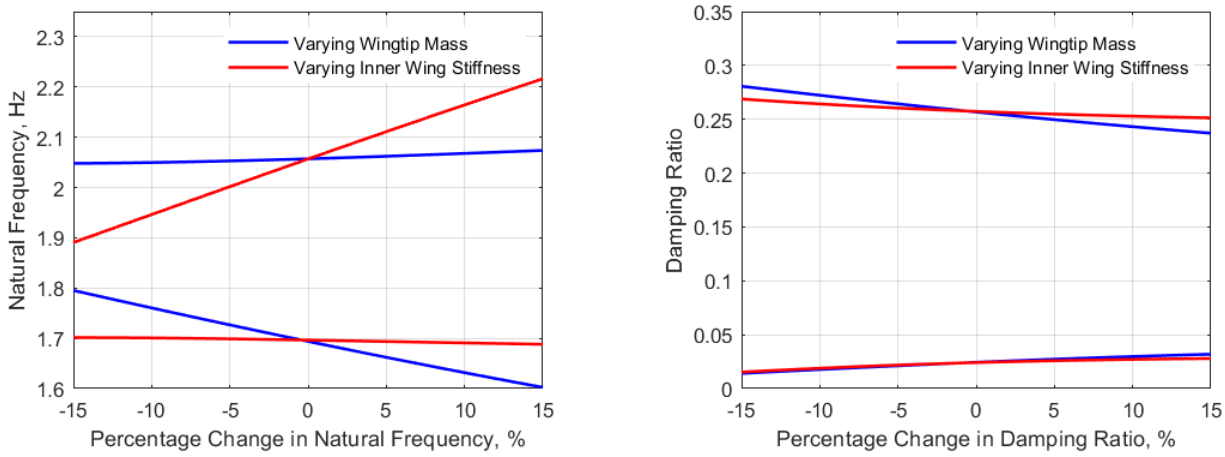

Figure 6: The results of the parameter study, changing wingtip mass and inner wing stiffness, at an angle of attack of 2.5 degrees, and an airspeed of 25 m/s. The natural frequencies and damping ratio's for both modes are shown on the graph.

Figure 6 shows that the natural frequencies are relatively sensitive to both parameters, and that at this condition, which is below the flutter onset speed for this angle of attack, the changes only significantly affect the mode they most relate too, with little change to the coupled characteristics. The natural frequency primarily for wing bending increases as stiffness increases, as expected, and as the wingtip mass increases, the natural frequency gets closer to the zero-airspeed natural frequency for this mode, again as expected, providing further validation to the model. The damping ratios don't deviate as much as these parameters are varied, however both damping ratios change when one of the parameters is changed, showing the coupling between the modes is more important for the damping characteristics.

3.2 Natural Frequency and Damping Ratio Analysis with The Ideal Control Surface Actuator

The active controller tested features two gains, a proportional gain K_p and a derivative gain K_d. The proportional gain has the effect of adding stiffness to the folding wingtip mode, while the derivative gain acts by adding damping to the wingtip mode, however this is a slight simplification as the wingtip forces due to the airflow are also affected to produce this effect.

The derivative gain was examined to see its effect on the wingtip flapping mode, and this was achieved by modelling the wingtip in isolation. At a fixed airspeed and angle of attack, the relationship between the derivative gain and wingtip damping coefficient was found to be entirely linear. Therefore, the remaining relationships can be examined by discussing how this gradient changes.

As angle of attack is varied, this gradient does experience some changes, however these are not significant, and so this gradient can be assumed to be constant as angle of attack changes. However, the effect of airspeed on this gradient varies greatly, and this relationship is shown in figure 7.

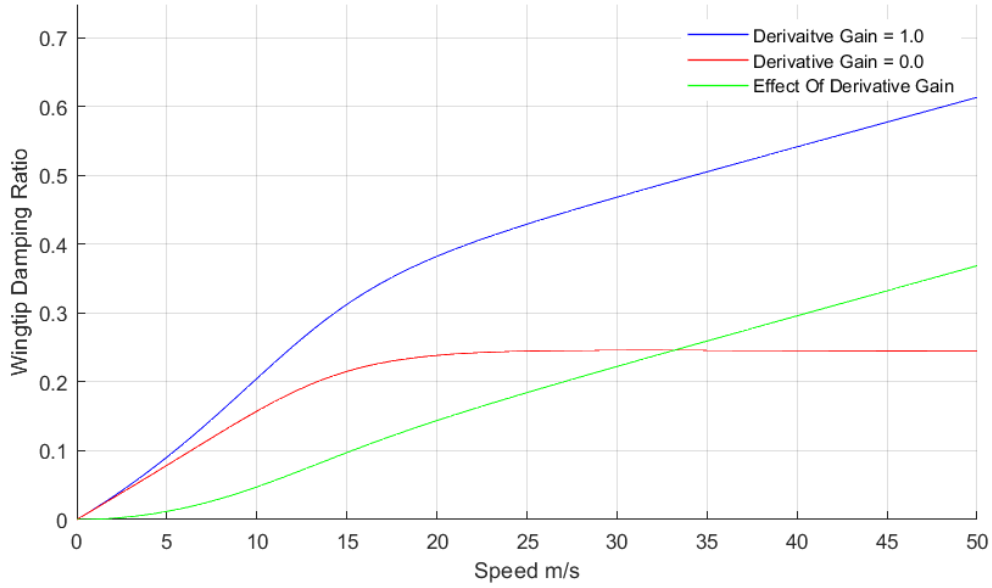

Figure 7: The difference in damping ratio when comparing a derivative gain of 0 and 1, on an isolated wingtip at an angle of attack of 2.5 degrees.

The increase caused by a derivative gain of one, shown on figure 7 as the '*effect of derivative gain'*, can be approximated to be a straight line for airspeeds above 10 m/s. As it can be approximated linearly, when assessed in isolation from the inner wing, an expression can be made to approximate the effect of adding a positive derivative gain on the wingtip damping coefficient ζ_{WT}, and can be shown to be equal to

$$\Delta\zeta_{WT} = (0.0078\,U - 0.0149)K_d \tag{16}$$

Now, returning to the full system, with the wingtip attached to the flexible inner wing, the effect of altering these gains on the natural frequency and damping characteristics of the system are examined. Figure 8 shows the effect of applying a proportional gain, $K_{p,}$ of 5.

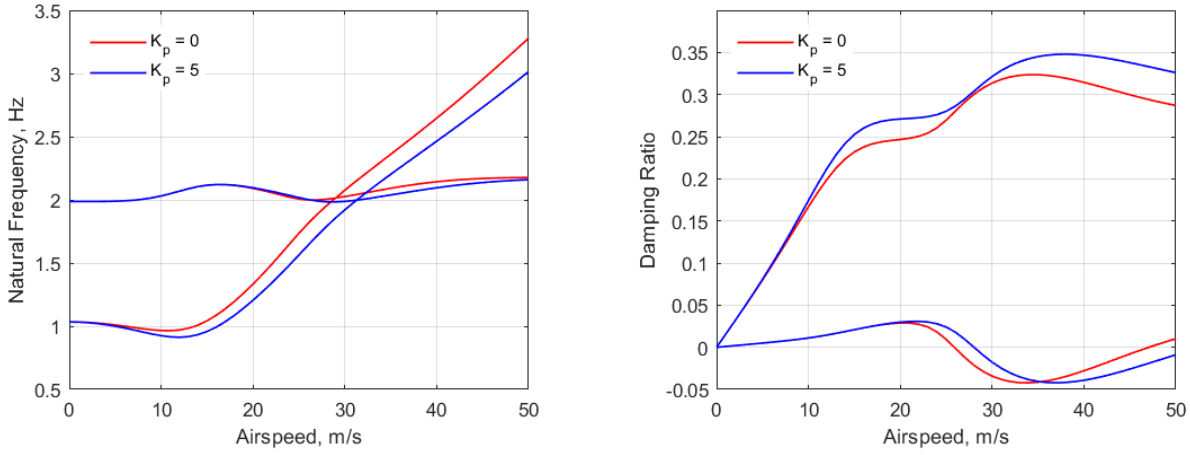

Figure 8: The effect of applying a proportional gain on the damping ratios and natural frequencies, at an angle of attack of 5 degrees.

As can be seen in figure 8, applying a proportional controller gain has no significant effect on the natural frequency associated primarily with inner wing bending, but delays the rise in the natural frequency primarily associated with the wingtip mode to higher airspeeds, pushing the point at which the two frequencies intersect to a higher airspeed. As these modes crossing is the primary flutter mechanism, this has the effect of pushing the flutter onset speed to a higher speed, which is the speed at which the damping ratio becomes negative, hence allowing the aircraft to operate to higher speeds before flutter occurs. The relationship between proportional gain and flutter onset speed, at a fixed angle of attack, is shown in figure 9.

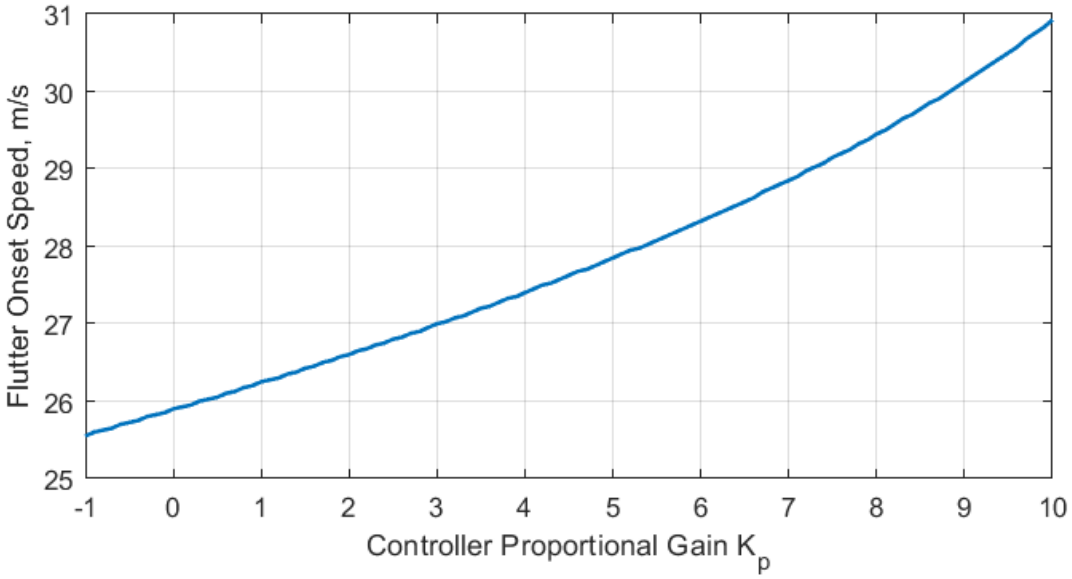

Figure 9: The effect of the controller proportional gain on the flutter onset speed, at an angle of attack of 5 degrees.

The use of a proportional gain is effective at pushing up the flutter onset speed, and therefore improving the stability characteristics of the wing. The gains examined were limited to -10 degrees, as using controller gains below this produces unrealistically high control surface deflection demands during a gust encounter. This shows that the proportional gain can push up the flutter onset speed by approximately 20%, however it cannot alleviate flutter completely.

The use of a non-zero flare angle creates a coupling between the local angle of attack of the wingtip and the wingtips current fold angle. As the control surface changes the zero-lift angle of attack, the use of a proportional gain creates a similar coupling. This was investigated by reducing the flare angle from 10 degrees to 5 degrees, and then adding a proportional controller gain to recreate the 10 degree flare angle results using the new model with a 5 degree flare angle. To determine if the effect had been matched, the equilibrium wingtip fold angle was considered as both airspeed and angle of attack were varied, as shown in figures 10 and 11, after a suitable controller gain had been identified.

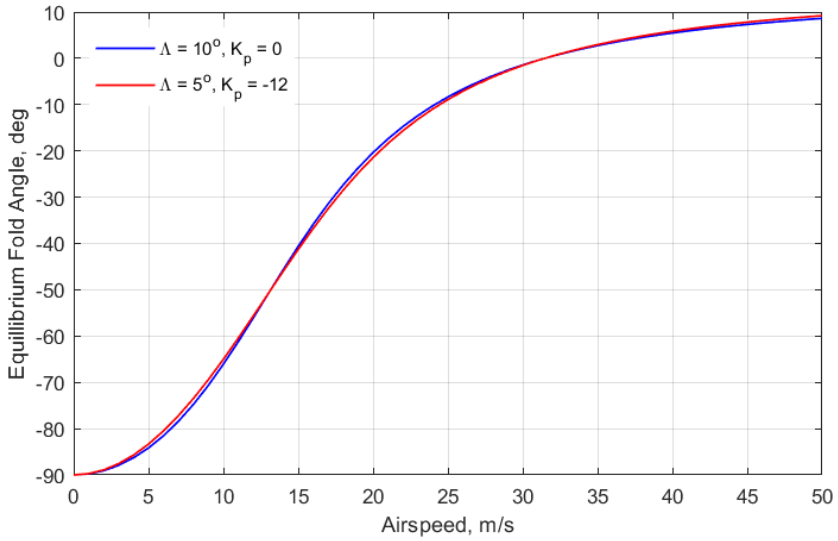

Figure 10 – The equilibrium fold angle as airspeed varies, at a constant angle of attack of 2.5 degrees, with the initial model, and the $\Lambda = 5^o$model with a proportional controller gain.

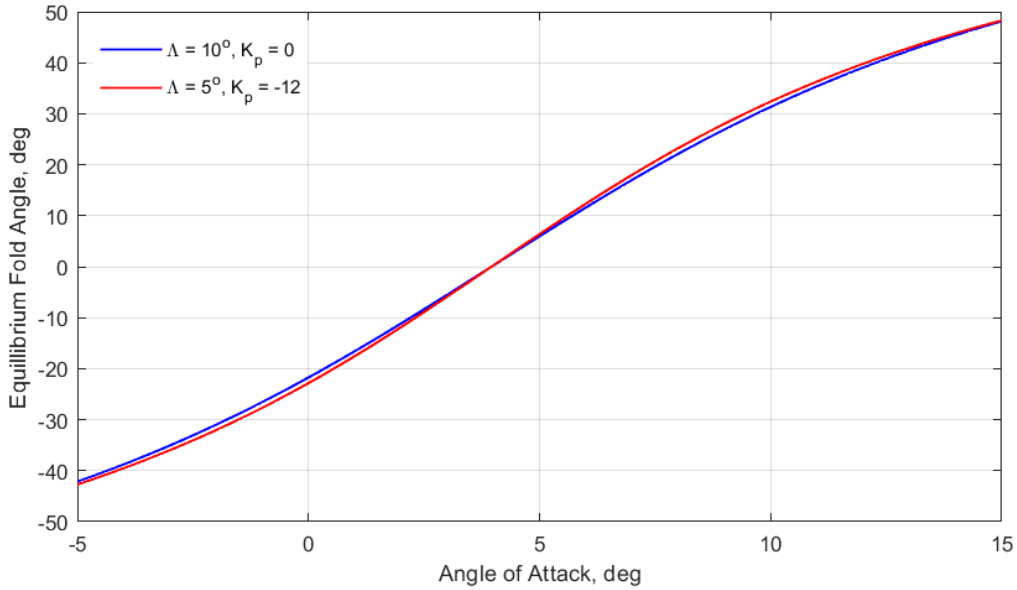

Figure 11 - The equilibrium fold angle as angle of attack varies, at a constant angle of airspeed of 25 m/s, with the initial model, and the $\Lambda = 5^o$model with a proportional controller gain.

These figures show that the required controller gain is independent of the aircrafts airspeed and angle of attack, which makes the system easier to implement. Figures 10 and 11 also show that the equilibrium positions can be matched almost exactly using a proportional controller gain. Therefore, this shows that the effective flare angle can be changed using a proportional controller, and therefore this allows tailoring of the effective flare angle during the flight.

To analyse the stability changes created by this change, the natural frequencies and damping ratios were analysed for both models, and these are shown in figure 12.

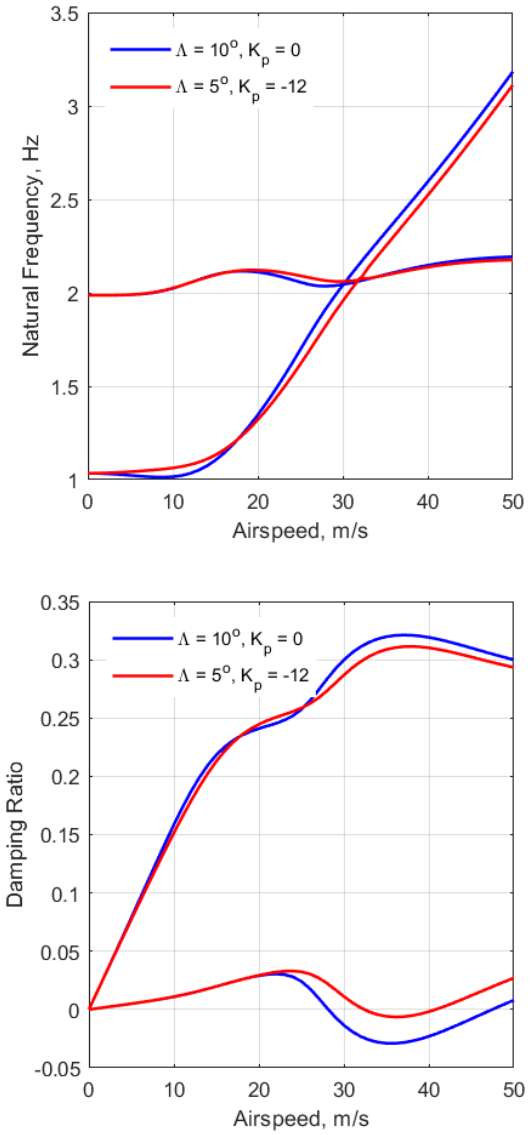

Figure 12 – The natural frequencies and damping ratios of the two models, at an angle of attack of 2.5 degrees.

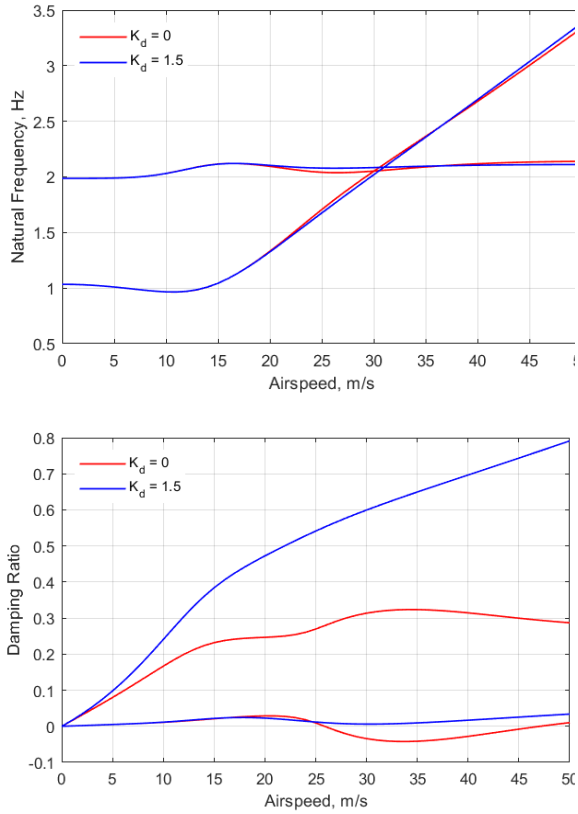

Figure 13: The effect of applying a derivative controller gain to the natural frequencies and damping ratios at an angle of attack of 5 degrees.

Figure 12 shows that, under the model using a proportional gain to recreate flare angle, the intersection of the natural frequencies is increased slightly. However, the hump mode created in the inner wing's damping characteristics is significantly reduced in magnitude, resulting in an increased flutter onset speed under the model using proportional gain to recreate the flare angle. The damping ratio of the wingtip mode is only slightly reduced. Additionally, by adding a slight derivative gain of 0.2, the model becomes stable at all airspeeds at this angle of attack.

By using a proportional gain to recreate the flare angle, flutter performance of the wing is significantly improved, and much lower derivative gains are needed to prevent flutter.

The other gain examined was the derivative gain K_d. Figure 13 shows the effect of applying this gain at a fixed angle of attack, and figure 14 shows just the critical damping ratio, that becomes unstable without a controller response, for multiple controller gains K_d.

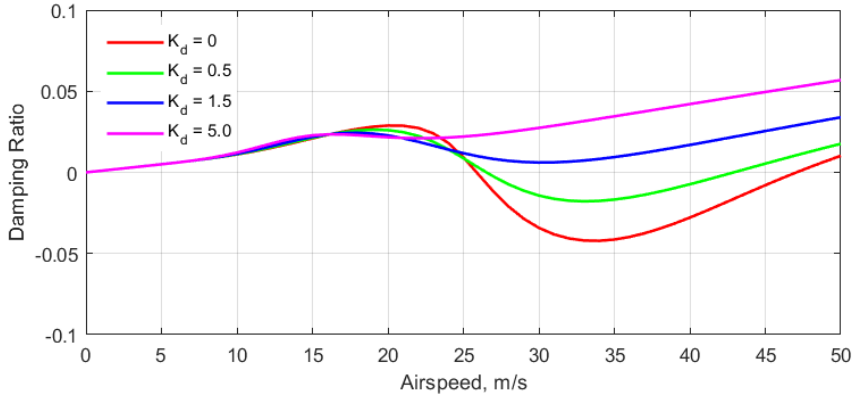

Figure 14: The effect of changing derivative gain on the critical damping ratio at an angle of attack of 5 degrees.

The results in figure 13 show that while applying a derivative controller gain has no significant effect on the natural frequencies of the system, it does have the slightly undesirable effect of gradually reducing the airspeed at which the two natural frequencies cross, which will slightly reduce the airspeed at which the minimum damping ratio is observed. However, as this is very gradual, this is not a particular cause for concern.

In contrast, the effects on the damping characteristics of the model by adding a derivative gain are much more significant. As expected, adding a derivative gain significantly increases the damping ratio for the mode primarily associated with the wingtip folding DoF, as it creates an aerodynamic force opposing the motion of the wingtip.

As shown in figure 14, adding a derivative gain also influences the damping ratio for the mode primarily associated with inner wing bending, particularly around the unstable section. This can be explained because the flutter occurs due to the interaction between the modes as the natural frequencies approach and then cross each other, meaning that in this region anything effecting the wingtip mode will also significantly affect the inner wing mode. In the natural response, there is a significant dip in damping ratio for the inner wing mode around the airspeed where the modes interact, however adding the derivative gain reduces this dip. In figure 14, it's shown that a derivative gain of 1.5 is sufficient to fully prevent the unstable behaviour at this angle of attack, and that a derivative gain of 5.0 almost completely removes the effect of this interaction on the inner wing damping ratio.

To examine the derivative gain necessary to fully prevent the onset of flutter, a parameter study was run where the effect of changing derivative gain was examined. In figure 15, this is presented as the derivative gain versus the minimum damping ratio seen across the range of possible airspeeds, where the possible airspeeds are those between 15 and 50 m/s. This was tested across multiple angles of attack, and these are presented as the different lines on the figure.

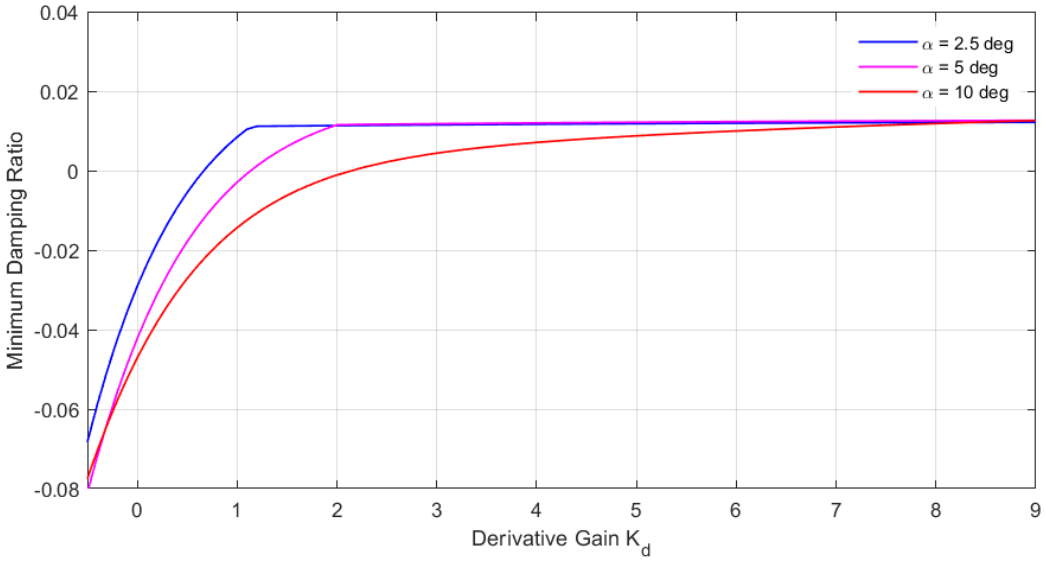

Figure 15: The effect of adding a derivative gain on the minimum damping ratio.

A negative damping ratio shows that flutter is present, whereas a positive damping ratio shows that any oscillations will instead gradually decay. As shown in figure 15, up to a certain point, increasing the derivative gain increases the minimum damping ratio, and allows flutter onset to be prevented. Above a certain point, adding additional derivative gain stops increasing the minimum damping ratio any further. At this point, the dip in damping ratio shown in figure 14 due to the interaction between the two modes has been eliminated.

As demonstrated when creating equation 16, the angle of attack has no significant effect on the change in damping ratio for an isolated wingtip due to controller derivative gain. Despite this, in the coupled system, there are significant differences as to how much derivative gain effects the damping ratio primarily associated with the inner wing mode as the angle of attack is changed, with the same derivative gain having less effect at higher angle of attacks. This coupled with the already more unstable system at higher angles of attack, which can be seen from the values of minimum damping ratio at zero derivative gain, means that the derivative controller gain required to prevent flutter increases significantly as angle of attack increases. Where flutter still occurs, the change in flutter onset speed due to derivative gain (below the gains required to fully prevent flutter) is minimal.

From the analysis of the effect of both proportional and derivative gain on the natural frequencies and damping ratios, proportional gains can be used to provide limited increases in the flutter onset speed, whereas the derivative gain can be used to fully prevent the onset of aircraft flutter, assuming the derivative gains required can be implemented.

3.3 Time Domain Response with the Ideal Control Surface Actuator

To assess whether these controller gains are feasible, the response of the model in the time domain needs to be considered. As one of the main use cases for wings fitted with FFWTs is for gust load alleviation, the gust response of the model was considered. At sea level, EASA specifies that the aircraft must be able to withstand gust with a maximum vertical velocity of up to 17.07m/s [16]. As the numerical model is based on a wing designed for wind tunnel testing, and not a passenger aircraft, then this value clearly must be reduced. The maximum gust velocity is roughly one quarter of a passenger aircraft landing speed, so the value used for gusts in these simulations was 25% of

the forward flight speed. Figure 16 shows the gust response of the model to a gust without active control being used, where the 1-cosine shaped gust starts 0.5 seconds into the simulation and is fully complete 1 second into the simulation.

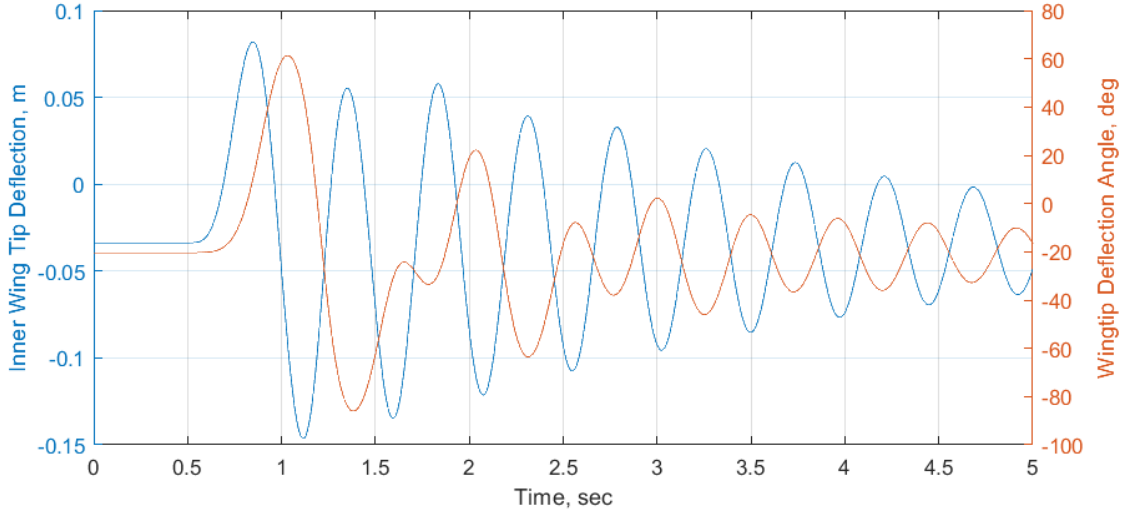

Figure 16: The natural response of the model to a 5m/s reference gust velocity, and gust length of 5m, during a 20 m/s flight speed, at a 2.5 degree angle of attack.

Figure 16 shows the interaction between the wingtip and wing bending mode of the model, and that once the gust has passed, they oscillate out of phase with each other. It also shows in the time domain the gradual damping out of the oscillations in both modes.

To consider how the control surface will respond to a gust encounter, the time domain response to the same gust as shown in figure 16 was considered for both a proportional gain of 10, shown in figure 17, and a derivative gain of 3, shown in figure 18. The derivative gain of 3 was selected, as this provides a positive damping ratio for all the examined angles of attack, as shown in figure 11.

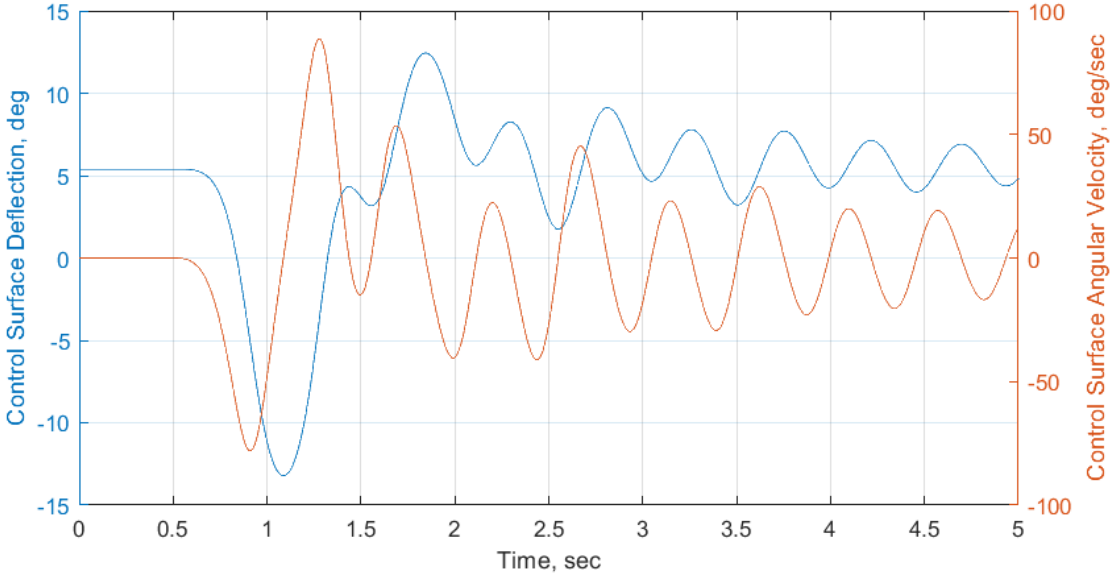

Figure 17: The control surface response under the same conditions as figure 16, with a proportional gain K_p of 10.

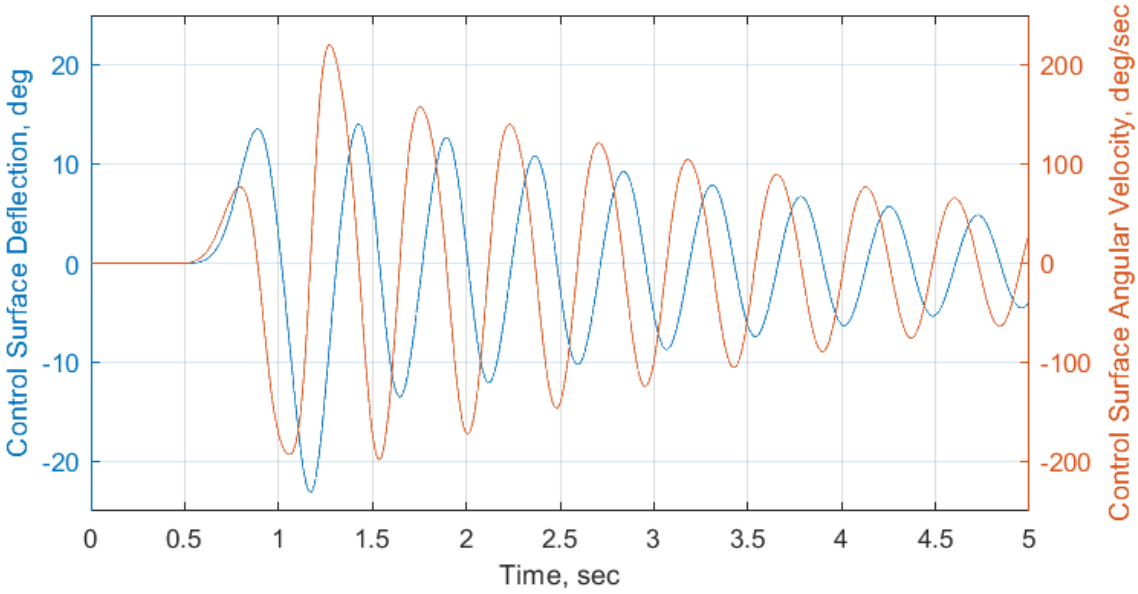

Figure 18: The control surface response under the same conditions as figure 16, with a derivative gain K_d of 3.

As can be seen in figures 17 and 18, under these conditions, the required control surface deflections are reasonable, and the maximum deflection limit of $\pm$ 30 degrees was never exceeded for either of the controller gains. However, due to the relatively large control surface deflections, and the relatively high frequency of the oscillations, the angular velocities experienced by the control surface are likely higher than what could be reasonably implemented. While this is true for both controller gains, with an angular velocity of 90 deg/sec likely being too high, the derivative controller scenario sees angular velocities exceeding 200 deg/sec. The angular velocities experienced did decay to a more reasonable rate over time, and it is mainly during the immediate aftermath of the gust encounter that they are unreasonably high. However, when operating above the flutter onset speed, the oscillations would grow instead of decay, so the system must be able to work enough to prevent flutter even at the large inner wing and wingtip oscillations initially experienced. The peak angular velocities experienced vary depending on the gust length encountered, and this relationship is shown in figure 19.

For this simulation, the peak gust vertical velocity has been reduced to 3 m/s. This is because for speeds larger than this, at some gust lengths, the maximum wingtip deflection exceeds 90 degrees when under a proportional gain, and therefore the model is no longer valid. Additional tailoring of the control logic could be used to prevent this happening, for example by reducing the control surface deflections once above a critical wingtip angle, however adding this non-linearity could affect the stability characteristics of the wing.

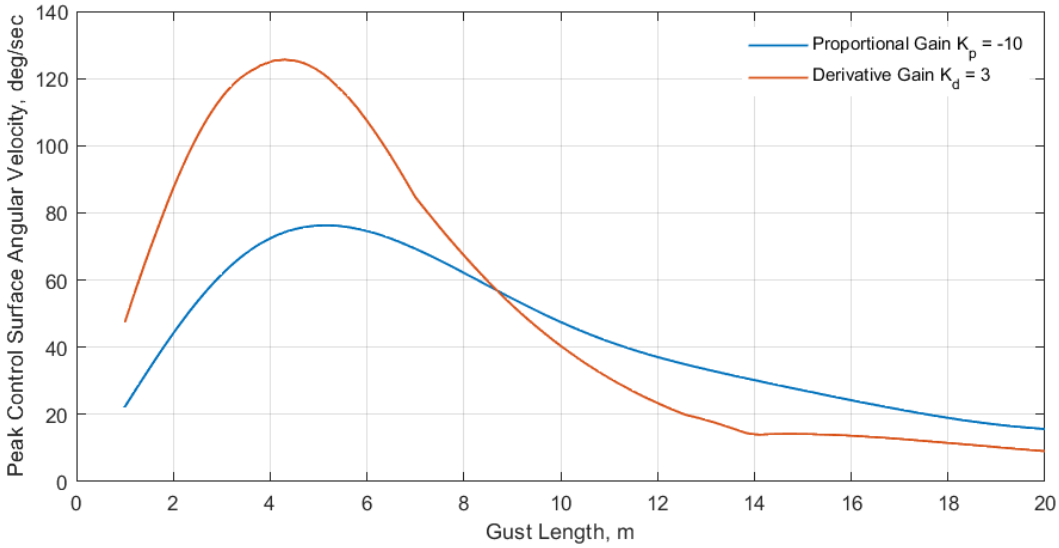

Figure 19: The peak control surface angular velocities as the gust length varies, under a vertical gust of 3m/s, forward flight speed of 20 m/s, and an angle of attack of 2.5 degrees, with both a derivative gain K_d = -10, and a proportional gain of K_p = 3 shown separately.

Figure 19 shows that the derivative gain produces the highest rotational velocities of the control surface, and that at low gust lengths these are high deflection rates, even at the reduced vertical gust of 3 m/s. It also shows that, for both controllers, the peak control surface deflection rates were observed during guest lengths of around 5m, as this corresponds with a 2 Hz gust frequency, which is the same as the inner wings natural frequency. As gust length increases, under both controllers the control surface angular velocities decrease and become much more reasonable. This shows that, while for larger gust lengths the angular velocities are reasonable, the demanded angular velocities at lower gust lengths could not be implemented in practice, and therefore it is necessary to examine the effect of limiting the control surfaces angular velocity on the wing's stability characteristics.

3.4 Wing Root Bending Moment with The Ideal Control Surface Actuator

The purpose of flared folding wingtips is to provide load alleviation, and therefore it is necessary to consider the impact that these controllers would have on the peak wing root bending moment (WRBM) observed during the gust encounter. Similarly to the control surface angular velocity, these will vary significantly as gust length varies. The model does not provide WRBM, however the degree of freedom for the inner wing deflection is an indicator of the relative amounts of WRBM experienced. Figure 20 shows the maximum change in inner wing deflection from the equilibrium position due to the gust encounter as the gust length is changed. To allow comparison to the natural response, the flight speed was selected to be below the natural flutter onset speed.

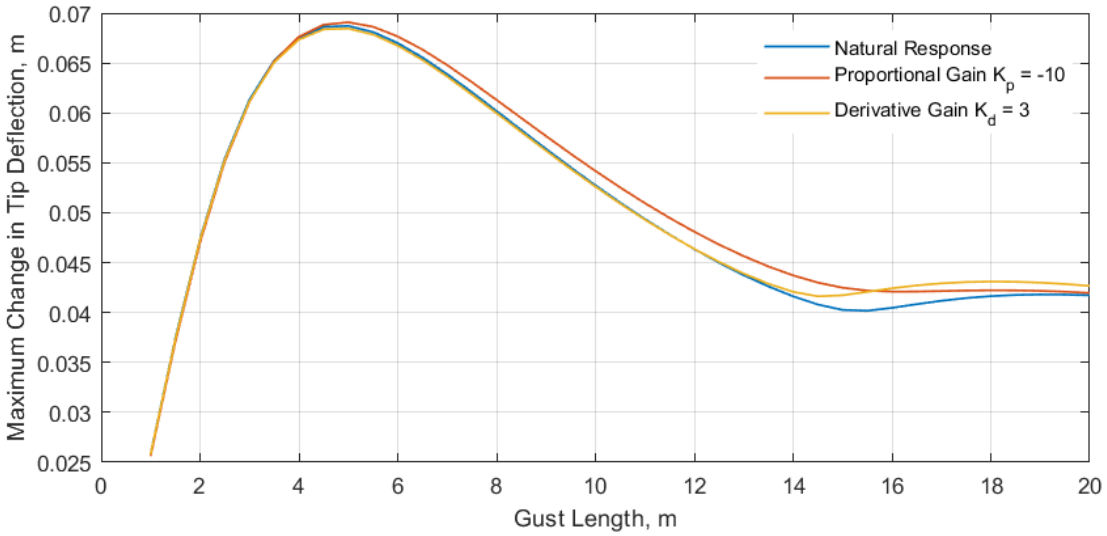

Figure 20: The effect of adding proportional and derivative control gains to the peak tip deflection from the equilibrium position, as gust length varies, under the same conditions as figure 19.

Figure 20 shows that adding a proportional gain increases the tip deflection due to the gust, and therefore the WRBM at all gust lengths. This is similar to results in previous research, which examined varying the hinge stiffness and found that a stiffness of zero provided optimal gust load alleviation [3]. Importantly, at the gust lengths where WRBM is highest, the increase in WRBM due to adding the control surface with proportional gain is small, and therefore the increased WRBM because of it is not that significant. As the gust length that produces the highest WRBM would be the design case for the wing structure, this also means that the increase in wing weight due to the slightly higher WRBM would not be significant.

The same logic also follows for the derivative gain, however here the peak change in tip deflection is slightly lower, but not by a significant margin. This means that there would be no increase in wing weight required due to the addition of a derivative gain. This result is expected, as the peak observed is due to the excitation of the aircrafts inner wing modes, and as such this gust length corresponds to a frequency of roughly 2 Hz, the inner wings natural frequency. As the derivative gain increases the inner wing damping ratio at these frequencies, then it is expected that the maximum deflection observed is reduced slightly by adding a derivative gain. At larger gust lengths, the response is much more dominated by following the gust, rather than the wings frequencies, and adding a derivative gain will reduce the maximum wingtip deflection, and therefore reduce the gust load alleviation effectiveness of the wingtip.

3.5 Time Domain Response with The Rate Limited Control Surface

As is shown in the above sections, the derivative controller was significantly more effective at flutter suppression, so only this is considered with the alternative control surface models.

Two time-domain simulations were run using the control surface, with an angular velocity limit of 50 deg/sec enforced. The first simulation was run to correspond with the same conditions as figure 17 above, allowing a comparison to be made. The control surface deflections, and velocities, associated with the gust encounter are shown in figure 21 below.

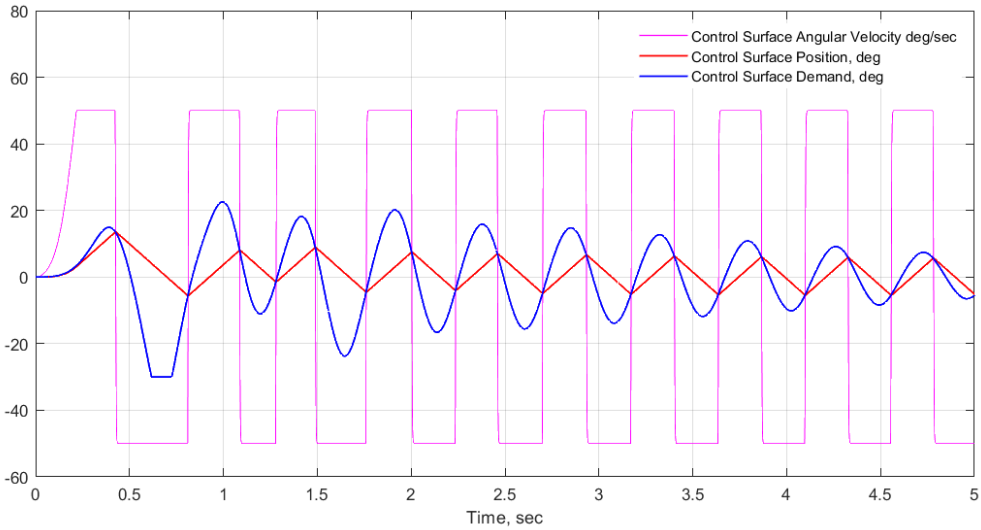

Figure 21: The control surface response of the rate limited control surface to a 5m/s reference gust velocity, and gust length of 5m, during a 20 m/s flight speed, at a 2.5 degree angle of attack, and a derivative gain $K_d = 3$.

The very high demanded angular velocities mean that, when a rate limit is imposed, the actual control surface angular velocity very quickly results in a square wave, rather than the sinusoid seen without the rate limit. This then has the effect of creating a triangular wave for the control surface deflection, instead of the sinusoidal demand signal applied. This triangular wave also features a significant phase shift from the input demand, which will affect the flutter suppression performance of the system. The maximum deflection amplitudes reached are also lower.

A limitation of this method of control surface simulation is that the almost square waveform for control surface angular velocities implies a near infinite acceleration on the control surface to achieve this, which is clearly not realistic. Additionally, this model does not account for any time delay due to the processing of the data. As there are obvious limitations in this model, it cannot be assumed to provide an accurate quantitative measure of the systems effectiveness, but it does provide a useful qualitative indication as to whether the demanded gains are realistic.

To examine whether these changes prevent the system from still being able to fully supress flutter, the second time domain simulation run with the rate limiter present was chosen to represent a reasonable worst-case scenario for the system. From figure 14, an airspeed of 32m/s was selected as a suitable worst-case airspeed, as this is where flutter onset is greatest. A high angle of attack of 10 degrees was also selected, to maximise the flutter present. Finally, the simulation to look at maximum demanded control surface velocity, as a function of gust length, was re-run to determine the gust length at these conditions that causes the maximum control surface velocity demand, which was found to be a gust length of 6.6m. The peak gust vertical velocity was increased to 8m/s, to keep it the same proportion of flight speed. The results of this simulation are presented in figure 22 below.

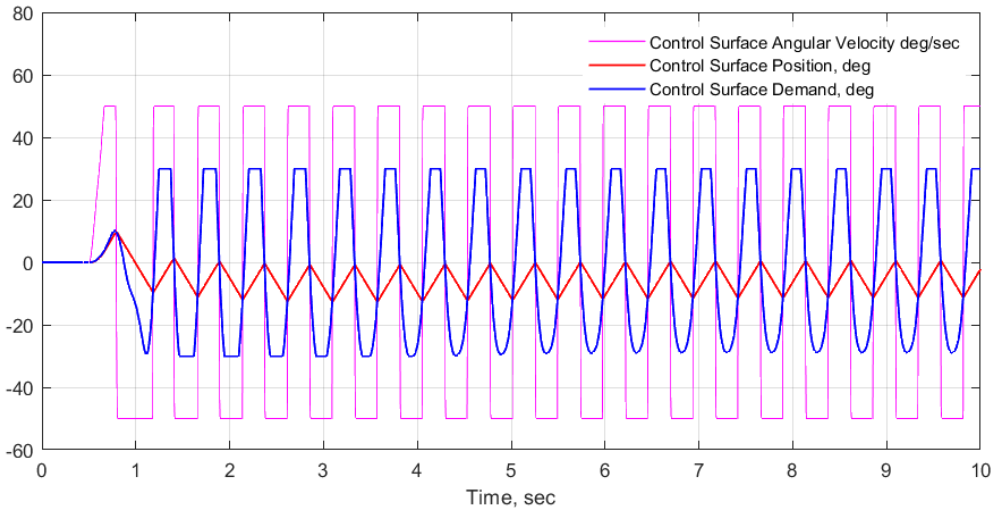

Figure 22: The control surface demand, position, and angular velocity over the simulation.

As expected, this simulation again features a triangular waveform for the control surface position, and a square waveform for the control surface velocity. The median control surface position becomes negative during this simulation, due to the more negative demands during the first couple of seconds of the simulation. Also, compared to the previous simulation, in this more extreme case, the phase difference between the demanded and supplied control surface deflection is now significantly greater, at almost 45 degrees, further reducing the control surface efficacy. To examine if the control system is still effective at preventing flutter, the response of the wing must be examined. As it is the mode that typically becomes unstable first, the inner wing tip deflection is presented in figure 23 below and is compared with that of the ideal control surface model.

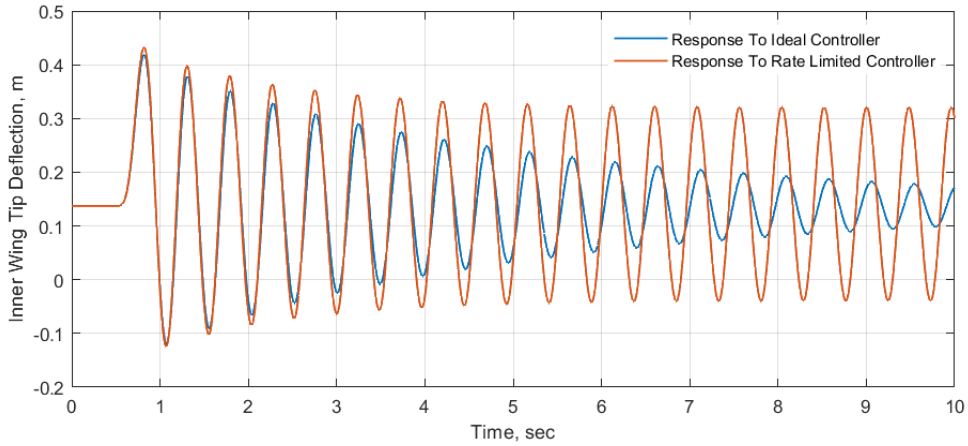

Figure 23: The Inner Wing Tip Deflection, comparing the result when simulating with both the ideal and rate limited control surface.

As shown in figure 23, the rate limited control surface performs very differently to the ideal control surface. The ideal control surface is effective at damping out the oscillations, whereas with the rate limited controller, the oscillations are not fully damped out, and instead enter a limit cycle oscillation. This is expected, as from looking at figure 22, as well as the phase shift, the demanded derivative gain is unable to be provided. At this worst-case scenario, an effective derivative gain of close to 3 must be provided by the system to adequately prevent flutter, and the far smaller

oscillations provided by the control surface are inadequate to do this. There is some positive effect of having the control surface present, as the positive deflection reached in the limit cycle is 0.321m with the controller active, compared to 0.332m under the natural response of the system. However, these oscillations are still too large for a limit cycle oscillation to be experienced safely in flight, as they have an amplitude of 0.18m on an inner wing only 0.875m long, therefore the system does not function sufficiently well under the reasonable worst-case scenario when using the rate limited controller model.

There are some design changes that could be made that may improve the performance of the system under the rate limited condition. The largest issues with this system occur with higher frequency oscillations, and so reducing the natural frequency of the oscillations would improve the performance of the control system. After the initial gust, the control surface is oscillating at the inner wing natural frequency, as this is the mode driving the behaviour after the gust has passed. In the parameter studies shown in figure 6, by reducing the inner wing stiffness, the natural frequency of the inner wing oscillations would be reduced, and hence the control surface would perform better. However, as wing stiffness is reduced the magnitude of the oscillations would be increased, so it is unclear if overall this would have a positive effect. Additionally, if a larger control surface was used, then the magnitude of the deflections needed to prevent flutter would be reduced, and therefore the control surface angular velocities demanded would also be reduced. However, this would come with a weight penalty.

3.6 Response with The Control Surface Actuator Model

Figure 24 shows the control surface response, using the actuator model instead of the rate limited model, under the same worst case scenario conditions described above.

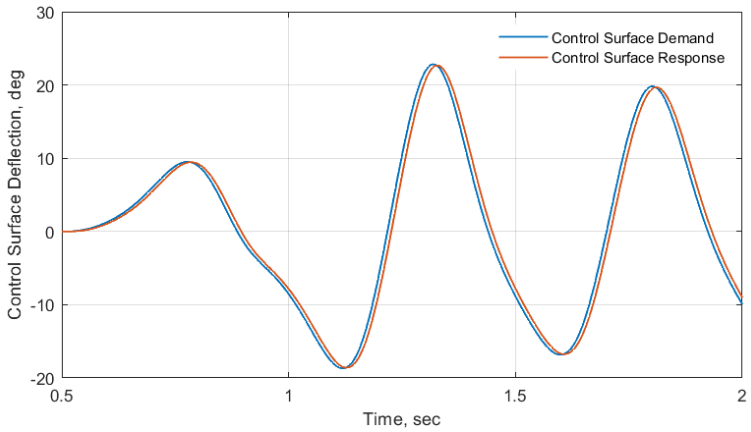

Figure 24: The control surface response using the control surface actuator model under the same conditions used to generate figure 22.

Figure 24 shows very little difference between the control surface demand and response induced by this actuator model. This is expected, as from the Bode plot of the transfer function, the phase difference at the 2Hz frequency is only -6 degrees. To examine the effect of this change on the model's behaviour, a calculation was run on the minimum damping ratio across the flight speeds, as derivative gain is changed, at a 10-degree angle of attack, following the same methodology as figure 15, and is shown in figure 25 below.

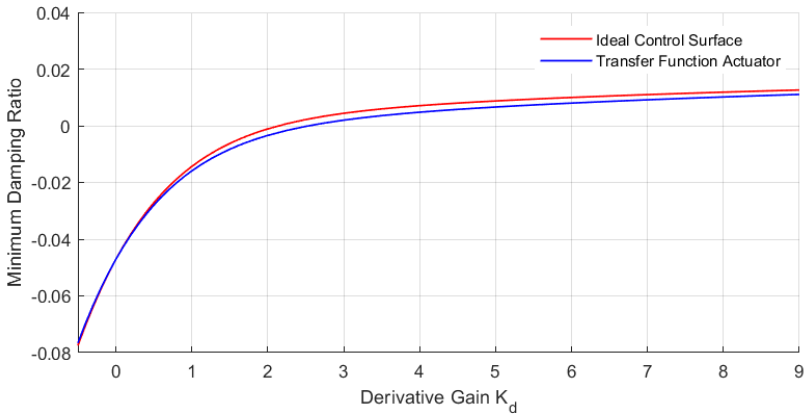

Figure 25: The effect of the transfer function for the actuator on the minimum damping ratio observed as derivative gain is changed.

As can be seen in figure 25, the non-ideal actuator does reduce the effect of the derivative gain when compared to the ideal control surface, however by using a slightly larger derivative gain, flutter suppression is still possible under this model at all points in the flight envelope.

However, this model is again not fully representative of a real control surface, as the high angular velocities observed are largely unchanged under this model compared to those for the ideal control surface. This means that under worst case gust loads the predicted performance under this model may not be achievable. Again, the flight control surface model used does not account for any controller delay, and therefore this is another factor that would likely reduce the flutter suppression performance in a real aircraft.

4 CONCLUSIONS

A two-degree of freedom model to represent a wing featuring flared folding wingtips (FFWT) was created, with an additional control tab on the wingtip. This controller used the wingtip deflection angle as an input signal, and the use of both proportional and derivative gains was investigated. Initially, an ideal control surface was used, where the control surface position was always the same as the demanded position. Using this ideal control surface, adding a proportional gain is effective at increasing the flutter onset speed by up to 5 m/s, by increasing the airspeed at which the wingtip flapping and inner wing bending modes cross. The use of a proportional gain was also shown that it could be used to change the effective flare angle of the wingtip. However, when using the ideal control surface model, adding a derivative gain was successful at fully preventing flutter at all reasonable airspeeds, and therefore was selected as the much more promising solution. For both the derivative and proportional controller gain, the benefits in preventing flutter, or increasing flutter onset speed, were achieved without any significant change to the amount of gust load alleviation provided by the FFWT.

However, these conclusions are built on the assumption of an ideal controller. This paper also showed that accounting for controller dynamics and nonlinearities such as limiting maximum control surface deflection and angular velocity can mitigate the observed benefits under worst case gust encounters.

Other dynamics which were considered in this paper are also likely of importance in considering the stability of these systems, such as the full dynamics of a control surface and considering the effects of controller delay and noise. Additionally, the simplification to a two degree of freedom model reduces the accuracy of the model, and so it is not known whether active control could cause instabilities in modes other than the wingtip flapping and first bending modes.

However, overall, the active control of a wingtip tab was shown to have significant influence on flutter mechanisms involving FFWTs meaning they are a potentially viable system to augment such instabilities.

REFERENCES

[1] T. Wilson, A. Castrichini, A. Azabal, J.E. Cooper, R. Ajaj, M. Herring, Aeroelastic Behaviour Of Hinged Wing Tips, *International Forum on Aeroelasticity and Structural Dynamics, Como, Italy, 2017*

[2] J.E. Cooper, J.R. Wright, Introduction to aircraft aeroelasticity and loads, Chapter 14, *Wiley, 2015*

[3] A. Castrichini et. al., Preliminary investigation of use of flexible folding wing tips for static and dynamic load alleviation, *The Aeronautical Journal, 121(1235), 2017, 73-94*

[4] Y. Chai, W. Gao, B. Ankay, F. Li, C. Zhang, Aeroelastic analysis and flutter control of wings and panels: A review. *International Journal of Mechanical System Dynamics, 1, 2021; 5-34*

[5] F. Healy, R. Cheung, D. Rezgui, J.E. Cooper, T. Wilson, A. Castrichini, On the Effect of Geometric Nonlinearity on the Dynamics of Flared Folding Wingtips, *Journal of Aircraft, 60:2, 2023, 368-381*

[6] F. Healy, R. Cheung, D. Rezgui, J.E Cooper, T. Wilson, A. Castrichini, Experimental and Numerical Nonlinear Stability Analysis of Wings Incorporating Flared Folding Wingtips, *Journal of Aircraft 61(1), 2024, 140-154*

[7] E. Cheung, D. Rezgui, J.E. Cooper, T. Wilson, Testing of Folding Wingtips for Gust Load Alleviation of Flexible High-Aspect-Ratio Wing, *Journal of Aircraft, 57(5), 2020, 876-888*

[8] E. Livne, Aircraft Active Flutter Suppression: State of the Art and Technology Maturation Needs, *Journal of Aircraft, 55(2), 2017, 1-41*

[9] The MathWorks, Inc. (2022). MATLAB version: 9.13.0 (R2022b). *Accessed: October 01, 2022. Available: https://www.mathworks.com*

[10] J. Case and A. H. Chilver, Strength of materials and structures: an introduction to the mechanics of solids and structures, *Chapter 21, Elsevier, 1999*

[11] P. McCreery, F. Healy, J.E. Cooper, Nonlinear Aeroelastic Behaviour of Flared Folding Wingtips During Gust Encounters, *Royal Aeronautical Society Applied Aerodynamics Conference, London, UK, 2022*

[12] F. Healy (2023), MOYRA (Multi bOdy dYnamics fRAmework), *accessed October 10th 2023, available at https://pypi.org/project/moyra/0.3.0/*

[13] XFLR5 (2019), version 6.47, *accessed 16th October 2023, available at https://www.xflr5.tech/*

[14] Pimentel-Garcia, J.C. The Full Multi-Wake Vortex Lattice Method: a detached flow model based on Potential Flow Theory, *Advances in Aerodynamics, 5:22, 2023*

[15] J. Case and A. H. Chilver, Strength of materials and structures: an introduction to the mechanics of solids and structures, *Chapter 13, Elsevier, 1999*

[16] European Union Aviation Safety Agency (EASA), Certification Specifications and Acceptable Means of Compliance for Large Aeroplanes (CS-25), CS-25.341, *Amendment 28, 2023, accessed 09/03/2024, available at https://www.easa.europa.eu/en/document-library/certification-specifications/cs-25*

[17] The MathWorks, Inc. (2019), ode1 solver, *accessed 01/04/2024, available at https://uk.mathworks.com/matlabcentral/answers/98293-is-there-a-fixed-step-ordinary-differential-equation-ode-solver-in-matlab-8-0-r2012b?#answer_107643*

[18] J. Theis, H. Pfifer, P. Seiler, Robust Control Design for Active Flutter Suppression, *AIAA Atmospheric Flight Mechanics Conference, San Diego, USA, 2016*

[19] F.Healy, H. Gu, D. Rezgui and J. E. Cooper, Nonlinear Stability Analysis of Floating Wingtips with Control Surface Freeplay,, *AIAA 2024-1267. AIAA SCITECH 2024 Forum. January 2024.*

COPYRIGHT STATEMENT